






## Determination of the optical bandgap of the Bernal and rhombohedral boron nitride polymorphs

Adrien Rousseau,<sup>1</sup> Matthieu Moret,<sup>1</sup> Pierre Valvin ,<sup>1</sup> Wilfried Desrat ,<sup>1</sup> Jiahua Li ,<sup>2</sup> Eli Janzen,<sup>2</sup> Lianjie Xue,<sup>2</sup> James H. Edgar ,<sup>2</sup> Guillaume Cassabois,<sup>1</sup> and Bernard Gil <sup>1,\*</sup>

<sup>1</sup>Laboratoire Charles Coulomb (L2C), UMR 5221 CNRS-Université de Montpellier, F-34095 Montpellier, France

<sup>2</sup>Tim Taylor Department of Chemical Engineering, Kansas State University, Manhattan, Kansas 66506, USA



(Received 15 April 2021; revised 21 May 2021; accepted 2 June 2021; published 16 June 2021)

We report a study of polymorphic boron nitride (BN) samples. We interpret the photoluminescence (PL) line at  $6.032 \pm 0.005$  eV that can be recorded at 8 K in  $sp^2$ -bonded BN as being the signature of the excitonic fundamental bandgap of the Bernal BN (bBN) [or graphitic BN (gBN)] polymorph. This is determined by advanced PL measurements combined with x-ray characterizations on pure hexagonal BN (hBN) and on polymorphic crystal samples, later compared with the theoretical predictions of Sponza *et al.*, [*Phys. Rev. B* **98**, 125206 (2018)]. The overall picture is consistent with a direct excitonic fundamental bandgap of the bBN (or gBN) polymorph. This value  $dX_b = 6.032 \pm 0.005$  eV is higher than the indirect bandgap of hBN ( $iX_h = 5.955 \pm 0.005$  eV).

DOI: [10.1103/PhysRevMaterials.5.064602](https://doi.org/10.1103/PhysRevMaterials.5.064602)

### I. INTRODUCTION

Boron nitride (BN) was synthesized by chemist Balmain [1] in the form of a white powder. Its individual microcrystals are typically flat, thin, and round or hexagonal platelets. It was established that several different BN phases or polymorphs can coexist, depending on their synthesis protocols and chemical environmental conditions [2–6]. There are specific stable periodic crystalline phases that were identified in the thermodynamic pressure-temperature phase diagram of BN, as represented by Fig. 2 of Ref. [7], among which are either  $sp^3$ -type or  $sp^2$ -type bondings. Atoms in the contexts of the noncentrosymmetric  $F\bar{4}3m$  ( $T_d^2$ ) cubic phase (cBN, borazone) and the noncentrosymmetric  $P6_3mc$  ( $C_{6v}^4$ ) wurtzite phase (wBN) are “fourfold”-coordinated, with  $sp^3$ -type bonding. There are many phases based on  $sp^2$  bonding, among which centrosymmetric, hexagonal BN (hBN) or white graphite [2]  $P6_3/mmc$  ( $D_{6h}^4$ ) is the most intensively studied; the noncentrosymmetric, rhombohedral BN (rBN)  $R\bar{3}m$  ( $C_{3v}^5$ ) is occasionally reported; and the Bernal (bBN) or graphitic (gBN) polymorph  $P\bar{6}2m$  ( $D_{3h}^3$ ) is least studied. The latter earns its name due to the similarity to the stacking sequence found in graphite. The hardness of the crystals under these various phases are very different [8,9]. Single-wall and multiwall BN nanotubes also exist [10].

Other phases, namely, pyrolytic BN (pBN) [11] and turbostratic BN (tBN) phases, are generally deposited by the reaction of ammonia and a boron halide under high temperature and high vacuum conditions, and they are formally analogous to turbostratic graphite [12]. They can be defined as trigonal  $B_3N_3$  hexagon layers stacked roughly parallel to each other, sometimes bent, with a random rotation and translation about the layer normal [13]. Crystallographic and

x-ray diffraction measurements indicate the presence of some two-dimensional ordering of atoms. For these phases, the  $c$ -lattice constant is larger than the value (0.333 nm) for the AA' (hBN) three-dimensional ordered stacking. The value of  $c$  is significantly increased in disordered crystals, reaching 0.356 nm in pure tBN. The average stack height  $L_c$  of a parallel layer group consists of four to five layers, while the average layer diameter  $L_a$  is much longer [13]. The structures of pBN and tBN are similar. Their difference is more or less of the order of semantics, most likely hidden under different degrees of the coherence length of the stack height  $L_c$  and the disorder of the orientational twist. The importance of all chemical actors contributing to the growth of the different partner phases at different steps of structural transitions between atomic ensembles with various degrees of disorder are reported in Ref. [14], as well as the interpretation of the global shape of the x-ray patterns and the values of  $c$  (measured as sitting in the 0.33–0.356 nm range) in terms of multiphase mixings [15]. The thermal transformation of tBN into the stable, hexagonal ordered layer lattice structure can be triggered by using ad hoc heat treatments [16].

Recently, interesting physical properties of tBN have been reported, among which are its high thermal conductivity [17], chemical stability at high temperature [18], and negative electron affinity [19], as well as the possibility to use it as a precursor for the growth of high-quality hBN. They have boosted it out of the laboratories of basic science into the application arena [20] at the same time as hBN was grown under the form of single crystals with millimetric sizes showing laser operation at 215 nm at room temperature [21,22].

hBN is the subject of abundant literature, and a full review is not within the scope here. Briefly, modern epitaxial growth methods can grow rather high-quality hBN films on a large variety of different substrates, including metals with high melting temperatures [23]. Its integration as a sacrificial layer for cleaving an light-emitting diode from its substrate

\*Corresponding author: [bernard.gil@umontpellier.fr](mailto:bernard.gil@umontpellier.fr)

is well established [24], as is the large-scale heteroepitaxy of hBN with transition-metal dichalcogenides [25]. Little attention has been dedicated so far to the epitaxial growth of rBN [26–29]. This polymorph results from a strong interaction with the growth substrate. Determining whether the deposited layer is the hBN or rBN polymorph is challenging, but it can be done by carefully interpreting accurate x-ray measurements (see Fig. 1 of Ref. [14], Table II of Ref. [29], and Fig. 6 of Ref. [30]). Even fewer studies have been dedicated to the Bernal polymorph.

The purpose of this paper is to propose an interpretation of photoluminescence (PL) measurements at 8 K as being the signature of the fundamental excitonic bandgap of bBN or gBN stacking, which is directly in reciprocal space with a value of  $dX_b = 6.032 \pm 0.005$  eV. This is higher than the indirect bandgap of hBN ( $iX_h = 5.955 \pm 0.005$  eV). To ensure the universality of our result, we studied samples of pure hBN and mixed phase crystals hBN/rBN/bBN in the hBN-rich composition range grown using different approaches.

The large number of hBN/rBN/bBN interfaces in our samples caused us to anticipate that measuring a consolidated value for the excitonic bandgaps of either bBN or rBN would not be easy, as the understanding of the origin of the PL of hBN has been cumbersome. It is dominated by defects with a broad band at 5.47 eV, and the indirect excitons that probe the indirect nature of the bandgap generally give weaker features at high energy. The strong and efficient interactions of excitons with phonons complicate the understanding of the light-matter interaction processes [31,32]. However, the indirect nature of the bandgap could be unambiguously demonstrated [32–34] after a series of high-resolution polarized PL experiments that revealed the well-marked phonon-assisted recombinations and the weak and tiny signature of the forbidden indirect exciton  $iX$  at 5.955 eV at 4 K [32,33].

This value is lower by 170 meV than the value of the direct bandgap obtained by a reflectivity experiment at 8 K:  $dX_h = 6.125$  eV [35]. This value for the bandgap is supported by the simultaneous complementary observation of phonon-assisted structures forming, at lower energy, a perfect mirror symmetry between phonon-absorption-assisted transitions (seen in reflectance) and phonon-emission-assisted transitions (seen in luminescence) around the  $iX_h$  energy position, both in energy and intensity [35]. The large energy splittings between 6.032 eV and these two values (5.955 and 6.125 eV) related to the hBN phase rule out any misleading contributions of inhomogeneous broadening effects. In addition, the value of the bandgap of the BN monolayer measured by PL is  $dX_{ml} = 6.080$  eV [36]; therefore, an artifact measurement on a delaminated monolayer piece of hBN is also ruled out.

## II. SAMPLES

The samples we study here are (001)-oriented flakes that were grown by precipitation from a metal solution, which led to very high-quality crystals. hBN crystals have been grown while testing a variety of solvents for their efficacy to produce high-quality large hBN flakes (pure Fe [25] and mixtures of Fe + Cr [37,38]), or carbon-doped hBN (Ni + Cr + C [39–41]). The solution was saturated with boron and nitrogen,

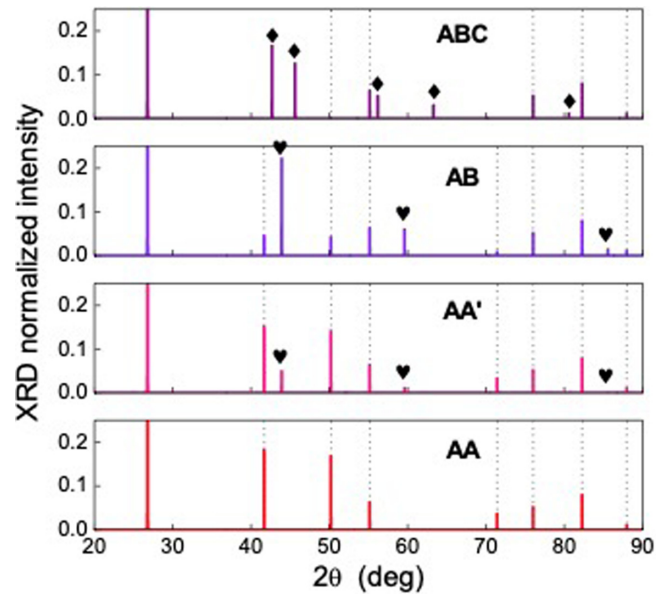


FIG. 1. Powder diffraction patterns computed for several boron nitride (BN) polytypes, with AA, AA', AB, and ABC stackings, from bottom to top. The intensity of the main peak at  $27^\circ$  is equal to unity for all phases. The x-ray source is copper.

then the BN was formed by precipitation during slow cooling ( $0.5$  to  $4^\circ\text{C/h}$ ) from  $1550^\circ\text{C}$  for  $25$  to  $50^\circ\text{C}$ .

Three types of samples were prepared.

(1) The standard growth used pure Fe as the solvent and hot-pressed BN as the boron source. The growth occurred in a  $\text{H}_2 + \text{N}_2$ -forming gas. This protocol permits us to obtain very high-quality monophase hBN crystals with large areas of defect-free material that micro-PL indicates to be almost free from impurities. This sample is labeled Fe, and the details of its growth are detailed in Ref. [25].

(2) A series of hBN were grown using iron plus vanadium, the latter element added to study its potential to enhance nitrogen solubility of the solution for producing thicker crystals. Here, the PL and x-ray diffraction characterization of a BN crystal grown from a 95% Fe + 5% V solvent mixture are reported. For this sample, elemental boron with the natural distribution of boron isotopes was the boron source. The growth also occurred in a  $\text{H}_2 + \text{N}_2$ -forming gas. This sample is labeled Fe + V.

(3) The third sample was grown with intentionally added carbon. The solvent was Ni + Cr, and the boron source was a mixture of 20%  $^{10}\text{B}$  and 80%  $^{11}\text{B}$ . A  $\text{CO} + \text{N}_2$  atmosphere was employed. Here, CO was used instead of hydrogen, to avoid etching of the carbon. This sample is labeled C + Ni + Cr.

## III. X-RAY MEASUREMENTS

We have plotted in Fig. 1 the theoretical relative intensities of the different diffraction peaks of BN powders, in the rBN (or ABC stacking), bBN (or AB stacking), hBN (or AA' stacking), and in the thermodynamically less stable hexagonal form (AA stacking) against the diffraction angle  $2\theta$ . The x-ray source is copper. The Miller indices are given for all

TABLE I.  $2\theta$  powder diffraction values of BN polytypes and their corresponding diffracting planes. The hexagonal (AA') and Bernal phases (AB) share the same  $2\theta$  angles. The indices of the rhombohedral (ABC) phase are given in the  $hk\ell$  hexagonal notation, in consistency with the other stackings. The x-ray source is copper.

$2\theta$ (deg.)	AA	AA'/AB	ABC
26.77	001	002	003
41.65	100	100	–
42.66	–	–	101
43.91	–	101	–
45.60	–	–	102
50.20	101	102	–
55.15	002	004	006
56.17	–	–	104
59.59	–	103	–
63.28	–	–	105
71.42	102	104	–
76.01	210	210	110
80.57	–	–	107
82.27	211	212	113
85.55	–	105	–
87.96	003	006	009

these polymorphs in the hexagonal representation in Table I. Obviously, many diffraction angles are common to all the polymorphs, and the distinction between rBN, hBN, and bBN phases in (001)-oriented crystals will not be possible, as the stacked planes diffract at the same angles:  $\sim 27^\circ$ ,  $\sim 55^\circ$ , and  $\sim 88^\circ$ . Interestingly, diffraction on slightly disoriented samples allows detection of complementary peaks indicated using diamonds for rBN and hearts for hBN and bBN at specific phase-discriminative angles in Fig. 1. The likely coexistence of the hBN and bBN polymorphs in real multilayer samples makes their distinction extremely subtle.

Figure 2 represents a series of x-ray diffraction spectra which were recorded at room temperature, in the Bragg-Brentano configuration using a Bruker D8DISCOVER diffractometer with a VÅntec linear detector. To increase the detectivity, we have used a simple Göbel mirror resulting in a nonmonochromatic primary beam:  $[\text{Cu}(K\alpha_1 + K\alpha_2)]$  with some traces of  $\text{Cu}(K\beta)$  and  $\text{W}(L\alpha_1)$ . According to Refs. [14,28–30], Fig. 1, and Table I, the complex features overlapping in the  $40^\circ$ – $45^\circ$  region for sample C + Ni + Cr (plotted in green) are the evidence of the coexistence of hBN and rBN. They are not observed for Fe + V (red plot) or Fe (blue plot). In the case of purely oriented (001) films and in the  $\theta$ - $2\theta$  condition, as alluded to earlier in this paper, only (002), (004), and (006) diffractions are expected at  $\sim 27^\circ$ ,  $\sim 55^\circ$ , and  $\sim 88^\circ$  angles, respectively. Although the samples have been carefully removed from the eutectic solidified, they have been slightly folded, and this leads to the additional diffraction features, for instance, of the  $[hk0]$  type, thanks to the sensitivity of our experiment.

The departure from perfect Bragg-Brentano geometry and/or inclusions of small amounts of polymorphism can both lead to supplementary peaks [42]. This is illustrated in Fig. 3, which displays a magnification of the  $40^\circ$ – $47^\circ$  region for sample C + Ni + Cr. There are obviously disorientated parts

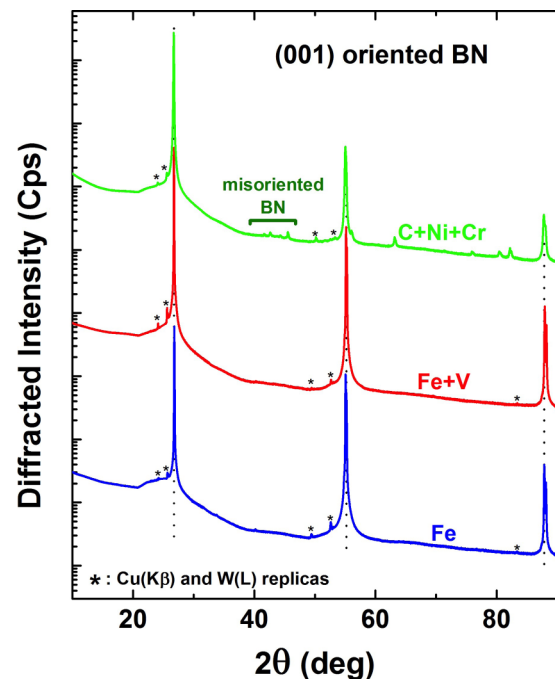


FIG. 2. From bottom to top, the x-ray diffraction  $\theta$ - $2\theta$  diffraction pattern recorded using  $\text{Cu}(K\alpha_1 + K\alpha_2)$  radiation ( $1.54186 \text{ \AA}$ ), for three highly (001)-oriented boron nitride (BN) Fe (blue), Fe + V (red) and C + Ni + Cr (green) samples. Asterisks correspond to the  $\text{Cu}(K\beta)$  ( $1.39222 \text{ \AA}$ ) and  $\text{W}(L\alpha_1)$  ( $1.47639 \text{ \AA}$ ) radiations. For C + Ni + Cr, lines supplemental of the  $\{(002), (004), (006)\}$  set are detected and plotted in dark green. The x-ray source is copper.

in the hBN crystal, as indicated on the one hand by the recording of the (100), (101), and (102) diffraction peak of hBN expected near  $41.66^\circ$ ,  $43.91^\circ$ , and  $50.20^\circ$ , respectively, and rhombohedral inclusions as evidenced by the recording of the (101) and (102) diffractions peaks of the rBN near  $42.66^\circ$  and  $45.60^\circ$ , respectively, at angles fitting with the prescriptions in Table I and in table II of Ref. [29]. This sample is a multiphase

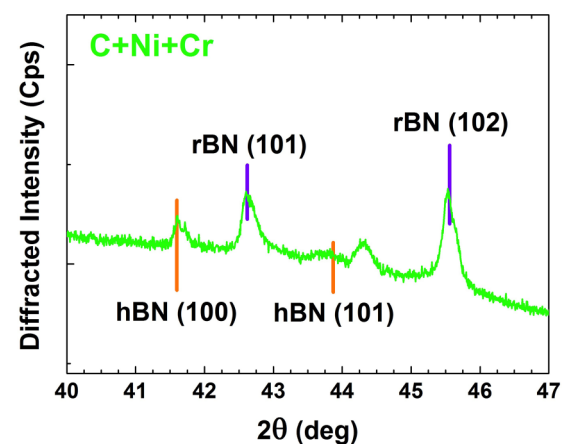


FIG. 3. Magnification of the diffraction feature in the  $40^\circ$ – $47^\circ$  region to show the existence of both hexagonal (hBN) and rhombohedral boron nitride (rBN) stackings. The structure at  $44.5^\circ$  is due to a residual of the Ni + Cr flux as well as a second one (not shown) at  $51.8^\circ$ . The x-ray source is copper.

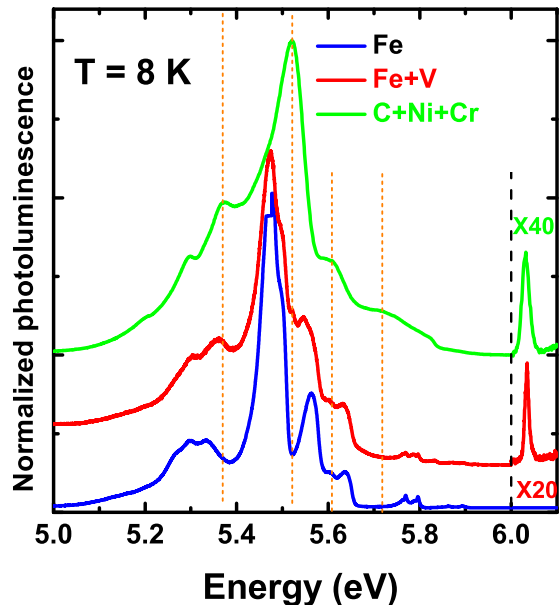


FIG. 4. The 8 K macro-photoluminescence (PL) spectra in the 5–6.1 eV range of several samples showing the phonon-assisted transitions typical of hexagonal boron nitride (hBN; blue spectrum), mixed with the undulations linked to rhombohedral boron nitride (rBN) inclusions overlapping with impurities (green and red spectra), as well as signature of the direct bandgap of Bernal boron nitride (bBN),  $dX_b$ , at 6.032 eV. We tentatively identify the 5.72 eV band in C + Ni + Cr as the unresolved analog of the  $iX_h$ -( $LO_T$  +  $TO_T$ ). Dashed orange lines are guides for the eyes.

crystal. There is no diffraction peak at  $26.30^\circ$  that would have proven the presence of tBN (Fig. 4 of Ref. [27]). Rocking curves are flat for the powder and for sample C + Ni + Cr, indicating a distribution of orientations. Rocking curves of Fe and Fe + V (not shown) are composite, made of distributed series of sharp peaks, a shape typical of high-quality layered compounds [38].

#### IV. PL

The PL is measured at liquid helium temperatures ( $T = 8$  K) in a closed-cycle cryostat with an excitation energy of 6.35 eV (195 nm) that is greater than the bandgap of BN. The optical setup consists mainly of a cw mode-locked Ti:Sa laser that produces an output power of 30  $\mu$ W, a Czerny-Turner monochromator equipped with an 1800-grooves/mm grating and a back-illuminated charge-coupled device camera for the detection. The lateral size of the laser spot at the sample surface is  $\sim 50$   $\mu$ m.

In Fig. 4 are gathered some low-temperature PL features collected in the 5–6.1 eV range. The spectra from the bottom to the top correspond to (i) a pure hBN crystal grown using  $^{nat}\text{B}$ ,  $\text{N}_2$ , and the Fe flux (Fe blue); (ii) hBN, grown again using  $^{nat}\text{B}$ ,  $\text{N}_2$ , and the Fe + V flux (Fe + V red); and (iii) the PL of the sample grown with carbon (C + Ni + Cr green).

The most intriguing features is the sharp transition noted  $dX_b$ , at  $6.032 \pm 0.005$  eV in samples Fe + V and C + Ni + Cr, and the weak structure at  $\sim 200$  meV below that is more clearly seen in the magnification of the 5.7–6.1 eV region in

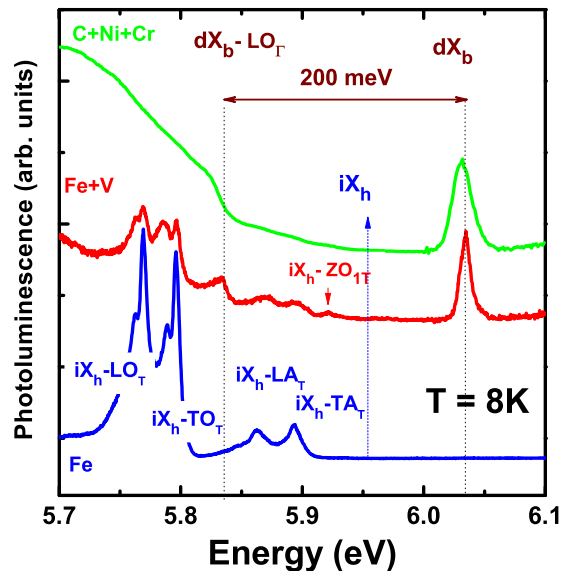


FIG. 5. Enlarged view of the 8 K macro-photoluminescence (PL) spectra in the 5.7–6.1 eV range that reveals the signature of the direct bandgap of Bernal boron nitride (bBN),  $dX_b$ , at 6.032 eV, as well as its 200 meV phonon-assisted replica (green and red spectra). In blue, the macro-PL of a high-purity hexagonal boron nitride (hBN) crystal. Transitions are labeled according to the convention in the literature. State  $T$  sits at the middle of the  $\Gamma K$  direction in the Brillouin zone of hBN.

Fig. 5, which is broader for C + Ni + Cr. This feature occurs at an energy of 5.83 eV, a value intermediate between the energy of the  $iX_h$ - $LA_T$  and  $iX_h$ - $TO_T$  phonon-assisted transitions of hBN. In addition, we disregard an overtone of the one phonon  $iX_h$ - $ZO_{1T}$ -assisted transition recorded at 5.93 eV with a complementary  $ZO_{1T}$  phonon at the middle (along the  $\Gamma K$  direction) of the Brillouin zone, thanks to intensity arguments and because we have not recorded it before when studying accurately the contributions of phonon symmetries in hBN [33]. In sample C + Ni + Cr, the high-energy side of this line is well resolved, like in Fe + V. The contribution of the many more defects to the global PL spectrum of this sample overlaps with its low-energy wing, thus unfortunately preventing us from clearly resolving it. From all these experimental arguments and from the lack of such a structure in our test sample Fe, we attribute this line as a phonon replica of the 6.032-eV line. The 200-meV splitting is energy and symmetry compatible with an LO phonon at  $\Gamma$ , which replicates efficiently thanks to the Frölich interaction process. The variation of the intensity and energy of the  $dX_b$  line slightly varies over the samples, and we safely frame its average value as  $6.032 \pm 0.005$  eV with a similar uncertainty as in hBN.

Since the  $dX_b$  transition at  $6.032 \pm 0.005$  eV cannot be recorded in high-quality hBN, it is the signature of a deviation from perfect AA' stacking. As we discuss in the last part of this paper, the sharp  $dX_b$  transition at  $6.032 \pm 0.005$  eV and the mechanism of replication with an  $LO_\Gamma$  phonon at zone center indicate the existence of bBN inclusions with a direct bandgap. Here, the bBN inclusions are embedded in an hBN material with an indirect bandgap, giving PL with many

phonon-assisted transitions involving phonons at the T point of the Brillouin zone.

## V. DISCUSSION

Although the existence of rBN inclusions was revealed by x-ray diffraction experiments, bBN was not detected. At this stage, the question of the PL signatures of tBN and rBN remain open. Back to the PL spectra, they globally display the same shapes, with similar kinds of broad undulations over the three samples. Some of these undulations are sometimes spectrally shifted (C + Ni + Cr) with respect to the ones traditionally recorded in hBN when the  $dX_b$  transition at 6.032 eV is not recorded (Fe). This indicates the evidence of a similarity among the differences that have been quoted by theoretical studies of the optical properties of hBN and rBN [43]. In the specific case of sample Fe + V, two interpenetrating series of undulations are detected, as seen in Fig. 4, the hBN-related series being far from the dominating one. We thus deduce that the optical signatures of hBN and rBN obtained from a simple PL experiment occur at different energies but overlap in a large energy range. We believe that the similarity of the shape of defect-related PL bands in hBN and rBN infer an indirect band structure for rBN, in contrast to bBN for which the bandgap is direct in reciprocal space. To consolidate this statement, we recall the PL of hBN, which is an unusual semiconductor in terms of light-matter interaction, as both extrema of the fundamental valence and conduction bands are sitting at different edges of the Brillouin zone [44–47]. The singularity of this material compared with other indirect bandgap materials resides in its specific indirect fundamental bandgap with the minimum of the conduction band sitting at the M point of the Brillouin zone, and the maximum of the valence band sitting in the close neighborhood of K. The PL that can be recorded in ultraviolet is based on spatially delocalized [48] one-phonon-assisted recombinations (phonons with an MK wave vector that translational symmetry brings equivalent to  $\frac{\Gamma K}{2}$ , that is to say a wave vector at the middle of the Brillouin zone along the  $\Gamma K$  direction) in the 5.7–5.9 eV range [31,32]. The energies of these transitions shift in samples monoisotopically pure in boron [33], as the phonon energies change when  $^{10}\text{B}$  or  $^{11}\text{B}$  are used instead of the natural boron ( $^{\text{nat}}\text{B}$  is made of 20%  $^{10}\text{B}$  and of 80%  $^{11}\text{B}$ ). In very high-quality crystals, the low-energy wings of the PL features are structured thanks to a complementary Raman scattering process involving the low-frequency ( $E_{2g}$ ) normal vibration mode [47]. Starting from 5.6 eV down to 5.3 eV or less, transitions localized to surface layer foldings with ad hoc sizes and orientation exist [48]. These localized emissions form a ladder of features, and they enhance the overtone featuring of the higher-energy phonon-assisted transitions [49,50]. They are neither observed in microcathodoluminescence [51] nor in micro-PL experiments [52] recorded in defect-free regions of hBN. They are the signature of complementary intervalley scattering assisted by TO(K-K') phonon modes [50]. The surface layer foldings permit us to simultaneously fulfill the requirements of the different conservation laws and offer the density of states required to bring the radiative recombination rate of Fermi's golden rule to substantial values that permits us to extract radiative recombination from the experimental

parasitic noise. Some contributions of recombination lines, namely,  $D_2$  and  $D_6$ , attributed to defects [50,53] and unidentified impurities [52] are also detected in this energy range, as well as more sophisticated many-impurity localization centers [54,55]. At energies <4 eV down to 1.5 eV roughly are a series of broad transitions attributed to still unknown impurities to boron-vacancy complexes. All of them operate as single-photon emitters, which indicates that hBN is a promising crystal for quantum technologies [23]. The global shape of the full PL spectrum revealing the strong exciton-phonon coupling [31,56] has been recently computed theoretically [57,58], as evidence of the degree of maturity reached in the understanding of the optical properties of hBN.

The broad undulating bands in all samples correspond to radiation by phonon-assisted carrier recombination, not to carriers localized to defects. The whole series of these phonon-assisted recombinations cascading from 5.955 eV down to 5.62 eV in hBN requires large areas of material, and features are observed at lower energies in defective areas. We believe that the crystalline quality of rBN as well as the density of defects prevents us from detecting similar effects here as the contributions of the different phases overlap (by the way, this statement also holds regarding the bBN inclusions) with the hBN-related features. From this, we derive the global energy shifts and PL shapes. Regarding the relative proportions of the different polymorphs, it is not easy to evaluate quantitatively.

There have been a few reports regarding the electronic structure of alternative stacking, like for instance, a Bernal (graphite) stacking or others [39,59–66]. Sponza *et al.* [43] have predicted a direct bandgap for bBN and indirect ones for hBN and rBN, with bBN having the highest value of the three and rBN the smallest. This paper offers some experimental confirmation of this, in terms of PL energies. The observation of a PL line  $dX_b$  (even tiny) at  $6.032 \pm 0.005$  eV supports the existence of bBN inclusions in the hBN. The replica redshifted by 200 meV can only be the energy of the so-called  $\text{LO}_3$  phonon branch at the zone center [57]. Because this phonon does not carry any wave vector and does not change the momentum balance in the recombination process, a replica involving this phonon either simply reproduces a sharp excitonic line, in the case the exciton is direct, or contributes to the formation of a series of lines that are redshifted by 200 meV with respect to the main series of phonon-assisted lines, in the case the exciton is indirect. In contrast to hBN, we do not observe here a complex series of lines either at  $\sim 6.03$  eV or at  $\sim 5.83$  eV, which strongly supports the direct nature of the recombination process giving rise to the PL signal at 6.03 eV in particularly good agreement with the accurate calculation of Ref. [44]. Still in the framework of Sponza *et al.* [43], who predict similarities between the phonon-assisted transitions and defect-related PL bands of rBN and hBN, and from the broad PL bands in sample Ni + Cr + C, we are inclined to tentatively suggest an indirect fundamental band structure for rBN. Unfortunately, this overlap of emission from different polymorphs prevents us from detecting the analog of the indirect exciton  $iX$  in hBN, which could not be unambiguously evidenced in our samples, in the range of energy proposed by Sponza *et al.* [43] ( $\sim 5.4$  eV). A pure rBN crystal should be required for that, which does not exist to date. This is

mandatory, as all the phonon modes being both infrared and Raman active, the set of phonon-assisted transitions is probably more documented than in the (already) complicated hBN case. Note that there has been a recent report for the optical value of the bandgap of tBN: 5.82 eV at room temperature, a value deduced from a Tauc plot analysis of transmission experiments [67]. The next question that comes to mind should be treated by theorists as it is: How are the band line-ups at the rBN-hBN interface, the bBN-hBN interface, and the rBN-bBN interface interconnected? Are they type I or type II? Are they both? Then based on the weak cross-talking of carriers photocreated in both phases and the apparent possibility to tune the density of rBN inclusions by growth conditions, it would become very tempting to envision extending the spectral range of single-photon emission operation limited to 4.1 eV [68] up to deep ultraviolet, at least at low temperature.

## VI. CONCLUSIONS

We have studied the optical signature at 8 K for bulk BN crystals that x rays indicate to be “pure” hBN and sometimes multiphase samples consisting of dominating hBN

contaminated by inclusions of rBN. Based on our preceding observation of an indirect excitonic bandgap  $iX_h$  at 5.955 eV and a direct one  $dX_h$  at 6.125 eV in hBN and on the determination of a direct excitonic bandgap at 6.080 eV in a monolayer of BN, we attribute a  $dX_b$  transition at 6.032 eV and its phonon replica 200 meV below the signature of the direct excitonic bandgap of a bBN stacking that is not discriminated by x-ray diffraction from the hBN one in our flake samples.

## ACKNOWLEDGMENTS

We gratefully acknowledge C. L’Henoret for his technical support at the mechanics workshop. This paper was financially supported by the network GaNeX (ANR-11-LABX-0014), the BONASPES project (ANR-19-CE30 0007), the ZEOLIGHT project (ANR-19-CE08-0016), and the Université de Montpellier. Support for BN crystal growth came from the Office of Naval Research, Award No. N00014-20-1-2474, and the National Science Foundation, Award No. CMMI #1538127.

- 
- [1] J. Thomas JR., N. E. Weston, and T. E. O’Connor, *J. Prak. Chem.* **27**, 422 (1842).
- [2] R. S. Pease, *Acta Cryst.* **5**, 356 (1952).
- [3] C. Coulson and R. Taylor, *Proc. Phys. Soc. A* **65**, 815 (1952).
- [4] R. H. Wentorf, *J. Chem. Phys.* **26**, 956 (1957).
- [5] H. J. Milledge, E. Nave, and F. H. Weller, *Nature* **184**, 715 (1959).
- [6] L. Zagyansky and G. V. Samsonov, *Журнал Прикладной Химии* **25**, 557 (1952); *J. Appl. Chem. U.S.S.R.* **25**, 629 (1952).
- [7] M. I. Petrescu and M. G. Balint, *U.P.B. Sci. Bulletin, Series B* **69**, 35 (2007).
- [8] M. I. Petrescu and M. G. Balint, *U.P.B. Sci. Bulletin, Series B* **69**, 43 (2007).
- [9] A. Polian, in *EMIS Datareviews Series*, edited by J. H. Edgar, S. Strite, I. Akasaki, H. Amano, and C. Wetzel (INSPEC, the Institution of Electrical Engineers, London, 1994), Vol. 23, p. 11.
- [10] N. G. Chopra, R. J. Luyken, K. Cherrey, V. H. Crespi, M. L. Cohen, S. G. Louie, and A. Zettl, *Science* **269**, 966 (1995).
- [11] A. W. Moore, *J. Cryst. Growth* **106**, 6 (1990).
- [12] J. Biscoe and B. E. Warren, *J. Appl. Phys.* **13**, 364 (1942).
- [13] N. E. Thomas Jr, Weston, and T. E. O’Connor, *J. Am. Chem. Soc.* **82**, 461 (1962).
- [14] M. G. Balint and M. I. Petrescu, *U.P.B. Sci. Bulletin, Series B* **69**, 79 (2007).
- [15] T. Matsuda, N. Uno, H. Nakae, and T. Hirai, *J. Mater. Sci.* **21**, 649 (1986).
- [16] S. Alkoy, C. Toy, T. Gönül, and A. Tekin, *J. Eur. Ceram. Soc.* **17**, 1415 (1997).
- [17] T. Sugino, S. Kawasaki, K. Tanioka, and J. Shirafuji, *Appl. Phys. Lett.* **71**, 2704 (1997).
- [18] K. P. Loh, I. Sakaguchi, M. N. Gamo, S. Tagawa, T. Sugino, and T. Ando, *Appl. Phys. Lett.* **74**, 28 (1999).
- [19] C. Kimura, T. Yamamoto, and T. Sugino, *Diam. Relat. Mater.* **10**, 1404 (2001).
- [20] T. K. J. Lian, X. Liu, J. Ma, and W. Zheng, *J. Phys. Chem. C* **113**, 9135 (2009).
- [21] T. T. Watanabe and H. Kanda, *Nat. Mater.* **3**, 404 (2004).
- [22] K. Watanabe, T. Taniguchi, T. Niiyama, K. Miya, and M. Taniguchi, *Nat. Photonics* **3**, 591 (2009).
- [23] B. Gil, G. Cassabois, R. Cusco, G. Fugallo, and L. Artus, *Nanophotonics* **9**, 3483 (2020).
- [24] Y. Kobayashi, K. Kumakura, T. Akasaka, and T. Makimoto, *Nature* **484**, 223 (2012).
- [25] J. Li, J. Wang, X. Zhang, C. Elias, G. Ye, D. Evans, G. Eda, J. M. Redwing, G. Cassabois, B. Gil, P. Valvin, R. He, B. Liu, and J. H. Edgar, *ACS Nano* **15**, 7032 (2021).
- [26] L. Xu, J. Zhan, J. Hu, Y. Bando, X. Yuan, T. Sekiguchi, M. Mitone, and D. Goldberg, *Adv. Mater.* **19**, 2141 (2007).
- [27] M. Chubarov, H. Pedersen, H. Högberg, J. Jensen, and A. Henry, *Cryst. Growth Des.* **12**, 3215 (2012).
- [28] M. Chubarov, H. Pedersen, H. Högberg, Z. Czigány, M. Garbrecht, and A. Henry, *Chem. Mater.* **27**, 1640 (2015).
- [29] M. Chubarov, H. Högberg, A. Henry, and H. Pedersen, *J. Vac. Sci. Technol., A* **36**, 030801 (2018).
- [30] X.-Y. Ren, C.-X. Zhao, C.-Y. Niu, J.-Q. Wang, Y. Jia, and J.-H. Cho, *Phys. Lett. A* **380**, 3891 (2016).
- [31] Y. Toyozawa, *Prog. Theor. Phys.* **20**, 53 (1958).
- [32] G. Cassabois, P. Valvin, and B. Gil, *Nat. Photonics* **10**, 262 (2016).
- [33] T. Q. P. Vuong, G. Cassabois, P. Valvin, V. Jacques, A. Van Der Lee, A. Zobelli, K. Watanabe, T. Taniguchi, and B. Gil, *2D Mater.* **4**, 011004 (2017).
- [34] T. Q. P. Vuong, S. Liu, A. Van der Lee, R. Cusco, L. Artus, T. Michel, P. Valvin, J. H. Edgar, G. Cassabois, and B. Gil, *Nat. Mater.* **17**, 152 (2018).

- [35] K. Watanabe and T. Taniguchi, *Phys. Rev. B* **79**, 193104 (2009), see, for instance, figs. 2(b) and 6.
- [36] C. Elias, P. Valvin, T. Pelini, A. Summerfield, C. J. Mellor, T. S. Cheng, L. Eaves, C. T. Foxon, P. H. Beton, S. V. Novikov, B. Gil, and G. Cassaboys, *Nat. Commun.* **10**, 2639 (2019).
- [37] S. Liu, R. He, Z. Ye, X. Du, J. Lin, H. Jiang, B. Liu, and J. H. Edgar, *Cryst. Growth Des.* **17**, 4932 (2017).
- [38] J. Li, C. Elias, Z. Ye, D. Evans, S. Liu, R. He, G. Cassaboys, B. Gil, P. Valvin, B. Liu, and J. H. Edgar, *J. Mater. Chem. C* **8**, 9931 (2020).
- [39] T. B. Hoffman, B. Clubine, Y. Zhang, K. Snow, and J. H. Edgar, *J. Cryst. Growth* **393**, 114 (2014).
- [40] J. H. Edgar, T. B. Hoffman, B. Clubine, M. Currie, X. Z. Du, J. Y. Lin, and H. X. Jiang, *J. Cryst. Growth* **403**, 110 (2014).
- [41] T. Pelini, C. Elias, R. Page, L. Xue, S. Liu, J. Li, J. H. Edgar, A. Dréau, V. Jacques, P. Valvin, B. Gil, and G. Cassaboys, *Phys. Rev. Mater.* **3**, 094001 (2019).
- [42] M. G. Balint and M. I. Petrescu, *Diam. Relat. Mater.* **18**, 1157 (2009).
- [43] L. Sponza, H. Amara, C. Attacalite, S. Latil, T. Galvani, F. Paleari, L. Wirtz, and F. Ducastelle, *Phys. Rev. B* **98**, 125206 (2018).
- [44] E. Doni and G. Pastori Parravicini, *Il Nuovo Cimento B* **64**, 117 (1969).
- [45] B. Arnaud, S. Lebegue, P. Rabiller, and M. Alouani, *Phys. Rev. Lett.* **96**, 026402 (2006).
- [46] P. Cudazzo, L. Sponza, C. Giorgetti, L. Reining, F. Sottile, and M. Gatti, *Phys. Rev. Lett.* **116**, 066803 (2016).
- [47] J. Koskelo, G. Fugallo, M. Hakala, M. Gatti, F. Sottile, and P. Cudazzo, *Phys. Rev. B* **95**, 035125 (2017).
- [48] R. Bourrellier, M. Amato, L. H. G. Tizei, C. Giorgetti, A. Gloter, M. I. Heggie, K. March, O. Stéphan, L. Reining, M. Kociak, and A. Zobelli, *ACS Photonics* **1**, 857 (2014).
- [49] T. Q. P. Vuong, G. Cassaboys, P. Valvin, V. Jacques, R. Cusco, L. Artus, and B. Gil, *Phys. Rev. B* **95**, 045207 (2017).
- [50] G. Cassaboys, P. Valvin, and B. Gil, *Phys. Rev. B* **93**, 035207 (2016).
- [51] L. Schué, L. Sponza, A. Plaud, H. Bensalah, K. Watanabe, T. Taniguchi, F. Ducastelle, A. Loiseau, and J. Barjon, *Phys. Rev. Lett.* **122**, 067401 (2019).
- [52] P. Valvin, T. Pelini, G. Cassaboys, A. Zobelli, J. Li, J. H. Edgar, and B. Gil, *AIP Adv.* **10**, 075025 (2020).
- [53] C. Attacalite, M. Bockstedte, A. Marini, A. Rubio, and L. Wirtz, *Phys. Rev. B* **83**, 144115 (2011).
- [54] S. F. Chichibu, Y. Ishikawa, H. Kominami, and Kazuhiko, *J. Appl. Phys.* **123**, 065104 (2018).
- [55] E. Tsushima, T. Tsujimura, and T. Uchino, *Appl. Phys. Lett.* **113**, 031903 (2018).
- [56] T. Q. P. Vuong, G. Cassaboys, P. Valvin, S. Liu, J. H. Edgar, and B. Gil, *Phys. Rev. B* **95**, 201202(R) (2017).
- [57] F. Paleari, H. P. C. Miranda, A. Molina-Sánchez, and L. Wirtz, *Phys. Rev. Lett.* **122**, 187401 (2019).
- [58] E. Cannuccia, B. Monserrat, and C. Attacalite, *Phys. Rev. B* **99**, 081109(R) (2019).
- [59] T. Galvani, F. Paleari, H. P. C. Miranda, A. Molina-Sanchez, L. Wirtz, S. Latil, H. Amara, and F. Ducastelle, *Phys. Rev. B* **94**, 125303 (2016).
- [60] D. Wickramaratne, L. Weston, and C. G. Van de Walle, *J. Phys. Chem. C* **122**, 25524 (2018).
- [61] K. Mengle and E. Kioupakis, *APL Mater.* **7**, 021106 (2019).
- [62] J. C. G. Henriques, G. B. Ventura, C. D. M. Fernandes, and N. M. R. Peres, *J. Phys.: Condens. Matter* **32**, 025304 (2020).
- [63] R. M. Ribeiro and N. M. R. Peres, *Phys. Rev. B* **83**, 235312 (2011).
- [64] L. Liu, Y. P. Feng, and Z. X. Shen, *Phys. Rev. B* **68**, 104102 (2003).
- [65] G. Constantinescu, A. Kuc, and T. Heine, *Phys. Rev. Lett.* **111**, 036104 (2013).
- [66] S. M. Gilbert, T. Pham, M. Dogan, S. Oh, B. Shevitski, G. Schumm, S. Liu, P. Ercius, S. Aloni, M. L. Cohen, and A. Zettl, *2D Mater.* **6**, 021006 (2019).
- [67] H. Yamada, N. Kumagai, T. Yamada, and T. Yamamoto, *Appl. Phys. Lett.* **118**, 112101 (2021).
- [68] R. Bourrellier, S. Meuret, A. Tararan, O. Stephan, M. Kociak, Mathieu, L. H. G. Tizei, and A. Zobelli, *Nano Lett.* **16**, 4317 (2016).